Nuclear magnetic resonance study of hydrogen diffusion in $HfV_2H_x(D_x)$ and $ZrV_2H_x(D_x)$: effects of phase transitions and isotope substitution

1991 J. Phys.: Condens. Matter 3 6277

(http://iopscience.iop.org/0953-8984/3/33/007)

J. Phys.: Condens. Matter 3 (1991) 6277–6291. Printed in the UK

Nuclear magnetic resonance study of hydrogen diffusion in $HfV_2H_x(D_x)$ and $ZrV_2H_x(D_x)$: effects of phase transitions and isotope substitution

A V Skripov, M Yu Belyaev, S V Rychkova and A P Stepanov
Institute of Metal Physics, Urals Branch of the Academy of Sciences, Sverdlovsk 620219, USSR

Received 19 September 1990

Abstract. Nuclear magnetic resonance measurements of ^1H and ^2D spin–lattice relaxation times in $HfV_2H_x(D_x)$ ($0.5 \leq x \leq 4$) and $ZrV_2H_x(D_x)$ ($1.1 \leq x \leq 5$) have been performed over the temperature range 11–420 K. The experimental results are analysed to obtain the H(D) diffusion parameters in the disordered (high-temperature) and the ordered (low-temperature) phases. Hydrogen ordering is found to have strong effects on the diffusion parameters. In the ordered phases of $HfV_2H_x(D_x)$ and $ZrV_2H_x(D_x)$ the experimental data can be described in terms of the model using a double-peaked distribution of activation energies E_a for hydrogen motion. This model implies the coexistence of two types of H(D) motion with different frequency scales. For both systems at $x > 3.5$ there is a distinct isotope effect in E_a for the disordered phase: $E_a^D < E_a^H$.

1. Introduction

The C15-type compounds HfV_2 and ZrV_2 absorb large quantities of hydrogen forming the solid solutions HfV_2H_x ($x \leq 4$) and ZrV_2H_x ($x \leq 5$). The notable feature of these systems is the broad homogeneity region spanning the whole accessible range of x at $T > 310$ K. This gives the opportunity to study the effects of hydrogen on the physical properties of these compounds without crossing phase boundaries. At $T < 310$ K, $HfV_2H_x(D_x)$ and $ZrV_2H_x(D_x)$ are known to exhibit a number of phase transformations [1–5]. The main features of the phase diagram of $ZrV_2H_x(D_x)$ studied by different techniques [5–10] appear to be established [8], although the structures of the low-temperature ordered phases are still unknown except for the one with $x \simeq 4$ [1, 2]. For $HfV_2H_x(D_x)$ data on the phase diagram are lacking; however, several lines of phase transitions have been determined from x-ray and NMR experiments [5].

Hydrogen diffusion in HfV_2H_x and ZrV_2H_x has been studied by Shinar *et al* [11] by NMR relaxation-time measurements. As in the other Laves-phase hydrides [12–14], the temperature dependences of ^1H spin relaxation rates in HfV_2H_x and ZrV_2H_x show strong deviations from the theoretical predictions based on the Arrhenius-type behaviour of hydrogen mobility. In order to account for these deviations the authors [11] invoked a model employing a continuous distribution of activation energies. While this approach seems to be natural for amorphous hydrides, the physical grounds of its application to crystalline compounds are not quite clear, especially in the case of ordered phases

0953-8984/91/336277 + 15 $03.50

with near-stoichiometric hydrogen content [15, 16]. The explicit relation between the activation energy and the pre-exponential factor invoked in [11] has also been questioned by Kirchheim and Huang [17]. The alternative model of hydrogen mobility in Laves-phase hydrides implies the coexistence of two types of motion with different frequency scales [12, 14]. Direct evidence for such a coexistence has recently been obtained from NMR measurements in the C15-type $TaV_2H_x(D_x)$ [18]. Since phase transitions in metal–hydrogen systems may strongly affect the hydrogen mobility, an accurate analysis of experimental data requires the knowledge of phase state and phase boundaries. Unfortunately, Shinar *et al* [11] have failed to take into account the effects of hydrogen ordering on diffusion parameters, relying on continuous fits to the data over wide ranges of temperature.

The aim of the present work is to study the microscopic features of H(D) motion in $HfV_2H_x(D_x)$ and $ZrV_2H_x(D_x)$ with special emphasis on the effects of phase transitions and isotope substitution. We have measured the ^1H and ^2D spin–lattice relaxation times T_1 in these systems over wide ranges of temperature, H(D) content and resonance frequency. The experimental data are analysed to obtain the H(D) diffusion parameters in the ordered and disordered phases. We also discuss the problem of the accurate determination of the electronic (Korringa) contribution to the spin relaxation rate and the peculiarities of H(D) diffusion in compounds with mixed-isotope composition. For compounds with $x \simeq 4$ the experimental results have been partially published in our previous papers [15, 16].

2. Mechanisms of spin–lattice relaxation

The measured spin–lattice relaxation rate T_1^{-1} in metal–hydrogen systems usually results from the sum of contributions due to conduction electrons (T_{1e}^{-1}) and hydrogen diffusion (T_{1d}^{-1}),

$$T_1^{-1} = T_{1e}^{-1} + T_{1d}^{-1}. \tag{1}$$

The electronic contribution is typically proportional to temperature, $T_{1e}^{-1} = CT$, and does not depend on resonance frequency ω. For protons the motional contribution T_{1d}^{-1} originates from dipole–dipole interactions between different ^1H spins (HH) and between ^1H spins and host-metal nuclear spins (HM). Using the standard equations [19], T_{1d}^{-1} can be expressed in terms of the spectral density functions for fluctuating dipolar fields. For the simplest model [20], known as the Bloembergen–Purcell–Pound (BPP) approximation, the spectral density functions are Lorentzian, and the motional contribution to the proton relaxation rate is given by

$$T_{1d}^{-1} = (T_{1d}^{-1})_{HH} + (T_{1d}^{-1})_{HM} = \frac{4}{3}\frac{M_{2H}}{\omega}\left(\frac{y}{4+y^2} + \frac{y}{1+y^2}\right)$$

$$+ \frac{1}{2}\frac{M_{2M}}{\omega}\left(\frac{y}{1+(1-\alpha)^2y^2} + \frac{3y}{1+y^2} + \frac{6y}{1+(1+\alpha)^2y^2}\right) \tag{2}$$

where $y = \omega\tau_d$, τ_d being the mean dwell time of a hydrogen atom in an interstitial site.

M_{2H} and M_{2M} are the contributions to the 'rigid lattice' second moment of the ^{1}H NMR line from HH and HM dipolar interactions, respectively, given by

$$M_{2H} = \tfrac{3}{5}\gamma_H^4\hbar^2 I_H(I_H+1)\sum_i r_i^{-6} \tag{3}$$

$$M_{2M} = \tfrac{4}{15}\gamma_H^2\gamma_M^2\hbar^2 I_M(I_M+1)\sum_j r_j^{-6} \tag{4}$$

where I_H and I_M are the spins, and γ_H and γ_M are the gyromagnetic ratios for H and M nuclei, respectively, and $\alpha = \gamma_M/\gamma_H$. The summations $\Sigma_i r_i^{-6}$ and $\Sigma_j r_j^{-6}$ refer to sums over hydrogen and metal sites, respectively, with the origin at a hydrogen site. All expressions apply to powder samples.

According to equation (2), T_{1d}^{-1} is expected to have a maximum when $y \simeq 1$. The precise value of y at which the T_{1d}^{-1} maximum is predicted depends on α and M_{2H}/M_{2M}. The maximum value of the relaxation rate, $(T_{1d}^{-1})_{max}$, is inversely proportional to ω. The asymptotic behaviour of T_{1d}^{-1} in the limits of fast ($y \ll 1$) and slow ($y \gg 1$) diffusion is given by

$$T_{1d}^{-1} \propto \tau_d \qquad y \ll 1 \tag{5}$$

$$T_{1d}^{-1} \propto \omega^{-2}\tau_d^{-1} \qquad y \gg 1. \tag{6}$$

If τ_d follows the Arrhenius relation,

$$\tau_d = \tau_{d0}\exp(E_a/k_B T) \tag{7}$$

where E_a is the activation energy for hydrogen diffusion, a plot of $\log T_{1d}^{-1}$ versus T^{-1} is expected to be linear in the fast-diffusion and slow-diffusion limits with slopes E_a/k_B and $-E_a/k_B$, respectively. It should be noted that more accurate lattice-specific calculations of the spectral density functions (see e.g. [21]) lead to results that are close to the BPP predictions. In particular, the asymptotic behaviour of T_{1d}^{-1} in the framework of lattice-specific calculations can also be written in the form of equations (5) and (6). For the studied $HfV_2H_x(D_x)$ and $ZrV_2H_x(D_x)$ systems the role of M nuclei is played by ^{51}V with $I_V = 7/2$ and nearly 100% natural abundance.

An important contribution to the ^{2}D spin–lattice relaxation rate may arise from the interaction of nuclear quadrupole moments with electric field gradients (EFG) modulated by deuterium diffusion. Since the gyromagnetic ratio of ^{2}D is considerably smaller than that of ^{1}H, the electronic and dipolar relaxation rates are less effective for ^{2}D, and ^{2}D relaxation in metal–deuterium systems is usually dominated by the quadrupolar contribution T_{1Q}^{-1}. In the studied C15 compounds the local symmetry of interstitial sites is non-cubic, and the EFG on ^{2}D is produced mainly by the neighbouring metal atoms. The corresponding quadrupolar contribution to the relaxation rate is expected to have the same temperature dependence as the dipolar deuterium–metal contribution [22, 23]. Hence, the temperature dependence of T_{1Q}^{-1} in the limits of fast and slow diffusion allows one to determine the activation energy for deuterium diffusion. However, the theoretical estimation of the maximum T_{1Q}^{-1} value is problematic since it requires knowledge of the spatial charge distribution and the antishielding factor for a given metal–hydrogen system. As has been noted by Seymour [22], it is also difficult to obtain a reliable estimate of τ_d at the temperature of T_{1Q}^{-1} maximum, especially if there are considerable contributions to EFG from the other deuterium atoms. Therefore, we shall analyse the ^{2}D relaxation data only to determine the activation energies.

Table 1. Compositions and lattice parameters of the studied $HfV_2H_x(D_x)$ and $ZrV_2H_x(D_x)$ samples at room temperature.

Sample	a_0 (Å)	Sample	a_0 (Å)
$HfV_2H_{0.5}$	7.450	$ZrV_2H_{1.1}$	7.549
$HfV_2H_{1.0}$	7.486	$ZrV_2D_{1.3}$	7.571
$HfV_2D_{1.3}$	7.526	$ZrV_2D_{2.0}$	7.653[a]
$HfV_2H_{1.9}$	7.585	$ZrV_2H_{2.4}$	7.690
$HfV_2D_{2.1}$	7.604	$ZrV_2D_{3.1}$	7.760
$HfV_2H_{3.2}$	7.700	$ZrV_2H_{3.4}$	7.773
$HfV_2D_{3.8}$	7.759	$ZrV_2D_{3.9}$	7.844
$HfV_2D_{3.9}$	7.775	$ZrV_2H_{4.0}$	7.860[a]
$HfV_2H_{4.0}$	7.780[a]	$ZrV_2D_{4.6}$	7.905
$HfV_2H_{0.5}D_{3.4}$	7.755	$ZrV_2H_{5.0}$	7.932
$HfV_2H_{1.5}D_{2.5}$	7.793	$ZrV_2D_{5.0}$	7.936
$HfV_2H_{3.0}D_{1.0}$	7.781	$ZrV_2H_{1.0}D_{3.0}$	7.848[a]
$HfV_2H_{3.4}D_{0.5}$	7.764	$ZrV_2H_{3.0}D_{1.0}$	7.860[a]

[a] At $T = 310$ K.

In some cases the motion of H(D) atoms cannot be characterized by a single τ_d value, i.e. a certain distribution of τ_d values exists in the system. Taking into account equation (7), the distribution of τ_d can be expressed as a distribution of E_a, and the motional relaxation rate is given by

$$T_{1d}^{-1} = \int T_{1d}^{-1}(E_a)G(E_a)\,dE_a \tag{8}$$

where $G(E_a)$ is the normalized distribution function of E_a values, and $T_{1d}^{-1}(E_a)$ is defined by equations (2) and (7). The application of equation (8) to calculations of the temperature dependence of T_{1d}^{-1} implies that the shape of $G(E_a)$ does not change with temperature.

3. Experimental details

The preparation of the samples of $HfV_2H_x(D_x)$ and $ZrV_2H_x(D_x)$ has been described elsewhere [4, 5]. X-ray diffraction studies have shown that at 310 K all the samples are single-phase solid solutions with the cubic C15-type host-metal structure. The compositions and lattice parameters of the studied samples are listed in table 1.

NMR measurements on powder samples were performed on a Bruker SXP pulse spectrometer at the frequencies $\omega/2\pi = 13.8$ MHz (^{2}D) and 19.3–90 MHz (^{1}H). Spin–lattice relaxation times were measured using the inversion-recovery method (pulse sequence 180°—τ—90°). In all cases the recovery could be fitted by an exponential function.

The low-temperature measurements were made in an Oxford Instruments CF1200 continuous-flow helium cryostat. The sample temperature monitored by a chromel/(Au–Fe) thermocouple was stable to within 0.1 K. For $T > 290$ K we used a glass Dewar system with an air flow. In this range the temperature monitored by a Cu/constantan thermocouple was stable to within 0.5 K.

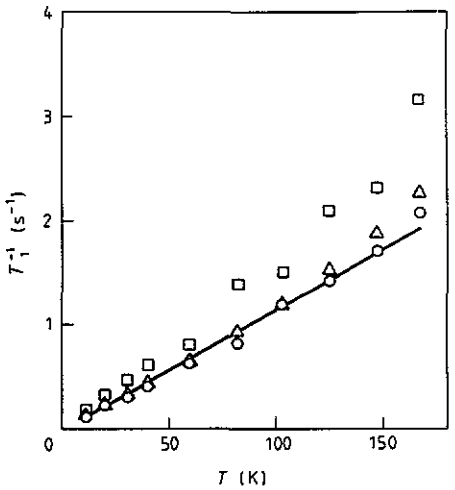

Figure 1. Low-temperature part of the temperature dependence of ^{1}H spin–lattice relaxation rates in $HfV_2H_{4.0}$ measured at (□) 34, (△) 64 and (○) 90 MHz.

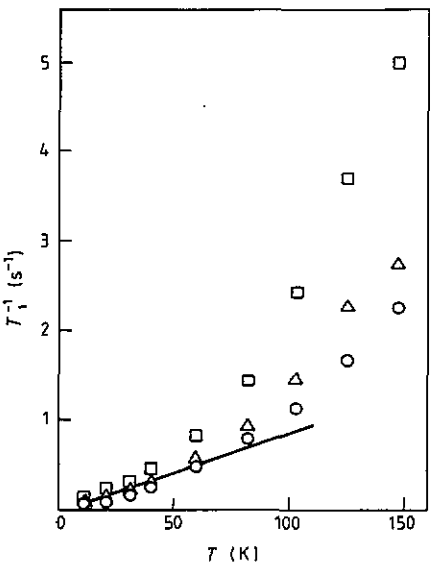

Figure 2. Low-temperature part of the temperature dependence of ^{1}H spin–lattice relaxation rates in $ZrV_2H_{2.4}$ measured at (□) 34, (△) 64 and (○) 90 MHz.

4. Results and discussion

4.1. Relaxation measurements at low temperatures

In order to analyse the spin–lattice relaxation data in terms of diffusion parameters, it is necessary first to separate the electronic contribution T_{1e}^{-1}. This contribution can be obtained directly from relaxation measurements in the low-temperature region where the diffusion is 'frozen', i.e. the motional contribution T_{1d}^{-1} is negligible. As examples of the observed temperature dependences of ^{1}H spin–lattice relaxation rates at low temperatures, we show in figures 1 and 2 the results of T_1^{-1} measurements in $HfV_2H_{4.0}$ and $ZrV_2H_{2.4}$ at three different frequencies. At $T < 40$ K the observed $T_1^{-1}(T)$ dependences are well approximated by the linear functions CT, the values of T_1^{-1} being nearly frequency-independent. Such behaviour is typical for the electronic contribution T_{1e}^{-1}. However, at higher temperatures considerable deviations from the linear $T_1^{-1}(T)$ dependence are found. Since these deviations are accompanied by the appearance of a marked frequency dependence of T_1^{-1}, they cannot be ascribed to changes in the electronic structure, but can be attributed to the onset of the motional contribution T_{1d}^{-1}.

Similar results have been obtained for the other studied samples of HfV_2H_x and ZrV_2H_x. It can be concluded that for an accurate determination of the electronic contribution T_{1e}^{-1} in HfV_2H_x and ZrV_2H_x it is necessary to measure T_1 down to very low temperatures and at sufficiently high frequencies. Even liquid-nitrogen temperature may be too high to determine T_{1e}^{-1} in these compounds. The frequency dependence of T_1^{-1} down to $T < 100$ K indicates that, even in this temperature range, hydrogen motion is not completely frozen on the NMR frequency scale. The paramagnetic impurity contributions to the ^{1}H relaxation rate appear to be negligible in the studied systems, since the low-temperature parts of $T_1^{-1}(T)$ dependences can be extrapolated to the origin.

Table 2. Electronic contributions to ^{1}H spin–lattice relaxation rates, $C = (T_{1e}T)^{-1}$, obtained from T_1 measurements at 90 MHz in the indicated temperature ranges.

Sample	$(T_{1e}T)^{-1}$ (10^{-2} s^{-1} K^{-1})	Temperature range (K)
$HfV_2H_{0.5}$	1.28	11–82
$HfV_2H_{1.0}$	0.70	11–82
$HfV_2H_{1.9}$	0.32	11–82
$HfV_2H_{3.2}$	0.47	11–60
$HfV_2H_{4.0}$	1.10	11–125
$ZrV_2H_{1.1}$	0.75	11–60
$ZrV_2H_{2.4}$	0.84	11–60
$ZrV_2H_{3.4}$	1.25	11–60
$ZrV_2H_{4.0}$	1.40	11–125
$ZrV_2H_{5.0}$	1.75	11–82

The values of $C = (T_{1e}T)^{-1}$ obtained from the proton T_1^{-1} measurements in the indicated temperature ranges are shown in table 2. These results have been partially published in [24, 25], where a discussion of the non-monotonic concentration dependence of $(T_{1e}T)^{-1}$ can be found. The electronic contribution to the proton relaxation rate in HfV_2H_x and ZrV_2H_x has also been studied by Shinar [26]. However, for most of the samples studied in [26] the T_{1e}^{-1} values have been obtained from relaxation measurements at $T > 77$ K. For some x our $(T_{1e}T)^{-1}$ values are lower than the corresponding data of Shinar.

4.2. Behaviour of relaxation rates near the temperatures of order–disorder phase transitions

For all the studied hydrides the temperature dependence of the proton T_{1d}^{-1}, obtained by subtracting T_{1e}^{-1} from the measured T_1^{-1}, shows a characteristic maximum. The same is also true for ^{2}D relaxation in the deuterides, the electronic contribution to the ^{2}D relaxation rate being estimated by scaling the proton T_{1e}^{-1} values for the corresponding hydrides by the factor $(\gamma_D/\gamma_H)^2$. Near the phase transition points additional features of the relaxation rate are observed. These features are particularly pronounced for the compounds with $x = 4$, where the H(D) content corresponds to the stoichiometric composition of the ordered δ-phase [1, 2], and the order–disorder transition is sharp. As examples of the observed behaviour we show in figures 3 and 4 the temperature dependences of T_{1d}^{-1} for ^{1}H and ^{2}D in $HfV_2H_{4.0}$, $HfV_2D_{3.9}$, $ZrV_2H_{4.0}$, $ZrV_2D_{3.9}$ and $ZrV_2H_{3.0}D_{1.0}$. If the transition point is close to the temperature of T_{1d}^{-1} maximum in the disordered phase, the observed maximum is 'folded'; in other cases there is a discontinuity in $T_{1d}^{-1}(T)$. The data presented in figures 3 and 4 indicate that the H(D) ordering is accompanied by the sharp increase in τ_d. This seems to be quite natural since the ordering is expected to result in the change in H(D) diffusion process. Indeed, in the disordered phase hydrogen can occupy at random a variety of interstitial sites of g-type (2 V + 2 Hf(Zr)) and e-type (3 V + 1 Hf(Zr)), while in the ordered phases of $HfV_2H_4(D_4)$ and $ZrV_2H_4(D_4)$ hydrogen is expected to jump over the almost completely filled sublattice including one-third of g-sites only [1, 2, 15].

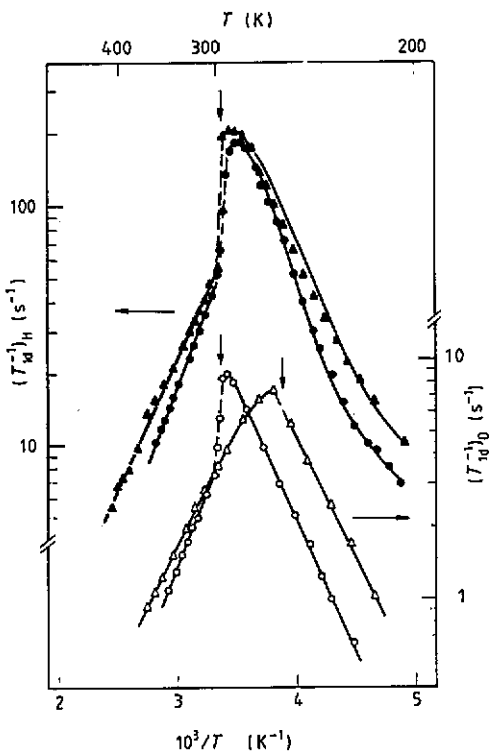

Figure 3. The motional contributions to the ^{1}H and ^{2}D spin–lattice relaxation rates in (▲) $HfV_2H_{4.0}$, (●) $ZrV_2H_{4.0}$, (△) $HfV_2D_{3.9}$ and (○) $ZrV_2D_{3.9}$ as functions of reciprocal temperature. The relaxation rates are measured at 19.3 MHz (^{1}H) and 13.8 MHz (^{2}D). The vertical arrows indicate the corresponding temperatures of order–disorder phase transitions. For $HfV_2H_{4.0}$ and $ZrV_2H_{4.0}$ at $T < 300$ K the full curves represent the fitting of the double-peaked model to the data (see section 4.4). All the other curves are guides to the eye.

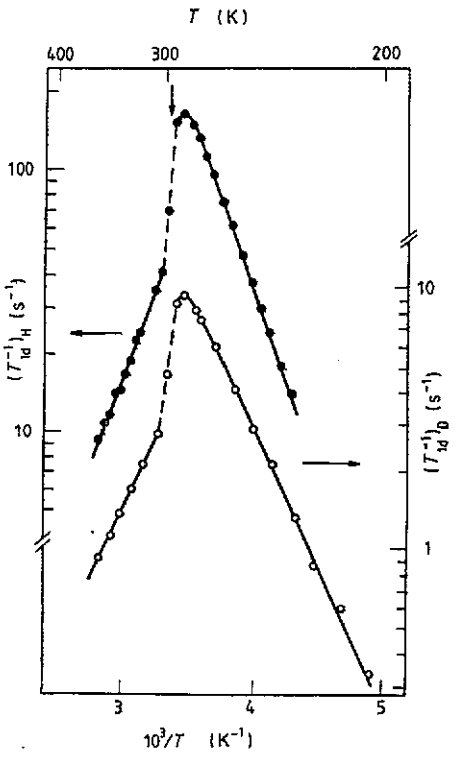

Figure 4. The motional contributions to the ^{1}H (●) and ^{2}D (○) spin–lattice relaxation rates in $ZrV_2H_{3.0}D_{1.0}$ as functions of reciprocal temperature. The relaxation rates are measured at 19.3 MHz (^{1}H) and 13.8 MHz (^{2}D). The vertical arrow indicates the temperature of the order–disorder phase transition. Full curves are guides to the eye.

The effects of order–disorder phase transitions on hydrogen diffusion in HfV_2H_x and ZrV_2H_x have not been taken into account in [11]. Although the discontinuity in T_1^{-1} near 300 K can be found in the raw experimental data of [11] for HfV_2H_4 and ZrV_2H_4, the results have been fitted by smooth curves calculated in the framework of the BPP model with the distribution of E_a. This approach leads to overestimated average values of E_a for the compounds with distinctly manifested phase transitions. For the compounds with $x \neq 4$ the effects of phase transitions on T_1^{-1} are weaker since the transitions are not very sharp. However, in all cases the diffusion parameters should be considered separately in the ordered and disordered phases. The concentration dependences of E_a in a wide range of x make sense only for the high-temperature (disordered) phase, since at low temperatures $HfV_2H_x(D_x)$ and $ZrV_2H_x(D_x)$ have a number of ordered phases with different stoichiometric compositions and structures [5, 6, 8]. On the other hand,

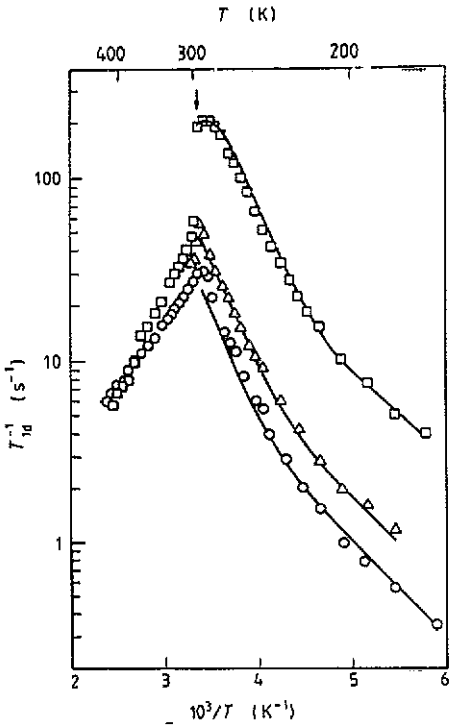

Figure 5. The motional contributions to the proton spin–lattice relaxation rates in $HfV_2H_{4.0}$ measured at (□) 19.3, (△) 61 and (○) 90 MHz as functions of reciprocal temperature. The arrow indicates the temperature of the order–disorder phase transition. The full curves represent the fitting of the double-peaked model to the data in the ordered phase (see section 4.4).

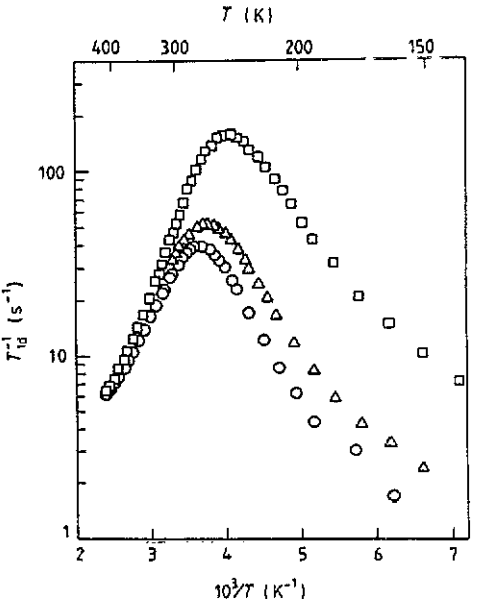

Figure 6. The motional contributions to the proton spin–lattice relaxation rates in $HfV_2H_{3.2}$ measured at (□) 19.3, (△) 61 and (○) 90 MHz as functions of reciprocal temperature.

as shown in [24], the effects of order–disorder transitions on the electronic structure parameters of $HfV_2H_x(D_x)$ and $ZrV_2H_x(D_x)$ are rather weak. Therefore, the use of the low-temperature $(T_{1e}T)^{-1}$ values for the disordered phase may be a reasonable approximation.

4.3. Parameters of H(D) diffusion in the disordered phase

Figures 3–8 show examples of the temperature dependences of T_{1d}^{-1} for ^1H and ^2D in a number of $HfV_2H_x(D_x)$ and $ZrV_2H_x(D_x)$ compounds. We consider first the general features of T_{1d}^{-1} data in the studied systems. (i) At high temperatures the dependence of $\log T_{1d}^{-1}$ on T^{-1} can be approximated by a linear function, as expected. (ii) The low-temperature slope of the $\log T_{1d}^{-1}$ versus T^{-1} plot is less steep than the high-temperature one. Moreover for some samples there is an additional break in the slope at low temperatures. (iii) In all the studied cases the frequency dependence of the maximum value of T_{1d}^{-1} goes as ω^{-1}. (iv) At low temperatures the frequency dependence of T_{1d}^{-1} goes approximately as $\omega^{-1.5}$, i.e. much weaker than the predicted ω^{-2} asymptotic

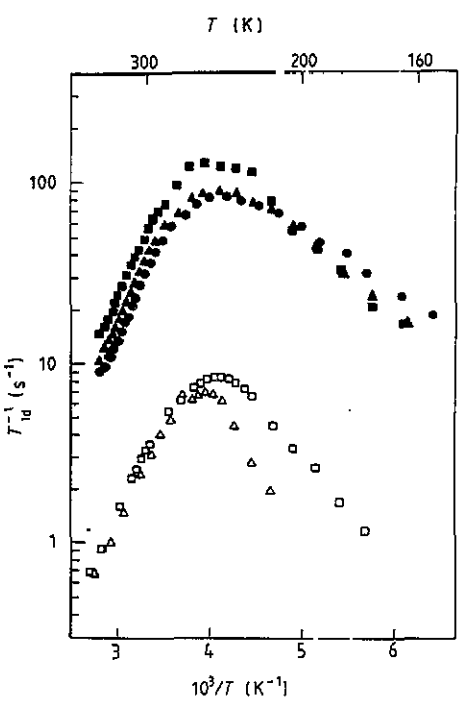

Figure 7. The motional contributions to the ^{1}H and ^{2}D spin–lattice relaxation rates in (●) $HfV_2H_{0.5}$, (▲) $HfV_2H_{1.0}$, (■) $HfV_2H_{1.9}$, (△) $HfV_2D_{1.3}$ and (□) $HfV_2D_{2.1}$ as functions of reciprocal temperature. The relaxation rates are measured at 20.5 MHz (^{1}H) and 13.8 MHz (^{2}D).

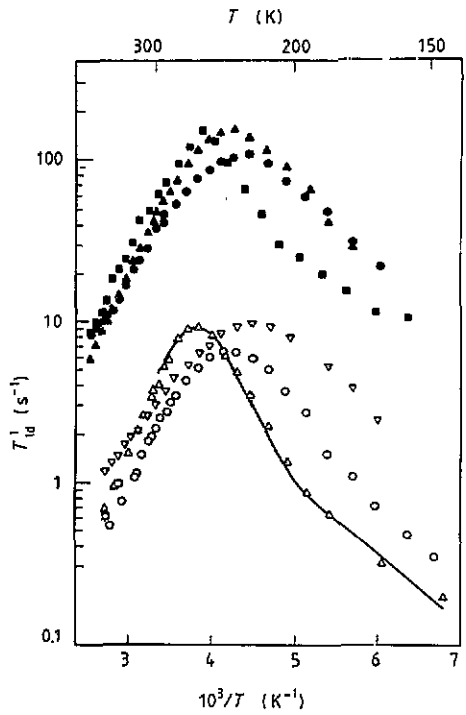

Figure 8. The motional contributions to the ^{1}H and ^{2}D spin–lattice relaxation rates in (●) $ZrV_2H_{1.1}$, (▲) $ZrV_2H_{2.4}$, (■) $ZrV_2H_{3.4}$, (○) $ZrV_2D_{1.3}$, (△) $ZrV_2D_{2.0}$ and (▽) $ZrV_2D_{5.0}$ as functions of reciprocal temperature. The relaxation rates are measured at 19.3 MHz (^{1}H) and 13.8 MHz (^{2}D). The full curve represents the fitting of the double-peaked model to the data for the ordered phase of $ZrV_2D_{2.0}$ (see section 4.4).

dependence. (v) The maximum value of T_{1d}^{-1} for ^{1}H increases strongly with increasing hydrogen content.

As noted in [14], feature (iii) is not consistent with the description based on a continuous τ_d distribution of considerable width. On the other hand, feature (iv) can hardly be explained without invoking some distribution of τ_d. Both these features may be described by the model using a double-peaked distribution of τ_d (or E_a) [14]. According to [14], the high-E_a peak of the distribution is expected to have a negligible width, and the low-E_a peak has a small amplitude and does not affect the relaxation rate behaviour at temperatures near and above the T_{1d}^{-1} maximum. Thus, at high temperatures the experimental data may be reasonably described in terms of the usual BPP model with a single E_a value. The resulting model parameters for the high-temperature phase of $HfV_2H_x(D_x)$ and $ZrV_2H_x(D_x)$ are shown in table 3 and 4 together with some experimental parameters. T_0 is the temperature of the lower boundary of the homogeneous solid solution region, i.e. below T_0 there is some kind of ordering or decomposition. The E_a values for the disordered phase have been determined from the slope of log T_{1d}^{-1} versus T^{-1} plots at high temperatures. The values of τ_{d0} have been

Table 3. Temperatures of phase transitions, T_0, and parameters of the motional relaxation of ^{1}H in the disorderd high-temperature phases. In the last four columns the observed and calculated values of $(T_{1d}^{-1})^{max}$ (including the contributions from HH and HV dipolar interactions) are listed.

Sample	T_0 (K)	$\omega/2\pi$ (MHz)	T_{max} (K)	E_a (eV)	τ_{d0} (s)	$(T_{1d}^{-1})^{max}_{obs}$ (s^{-1})	$(T_{1d}^{-1})^{max}_{calc}$ (s^{-1})		
							Total	HH	HV
$HfV_2H_{0.5}$	220	20.5	239	0.22	1.7×10^{-13}	85	245	17	228
$HfV_2H_{1.0}$	220	20.5	243	0.22	2.7×10^{-13}	92	252	30	222
$HfV_2H_{1.9}$	230	20.5	248	0.22	2.8×10^{-13}	130	259	54	205
$HfV_2H_{3.2}$	240	19.3	247	0.22	2.4×10^{-13}	157	285	87	198
$HfV_2H_{4.0}$	297	19.3	290	0.22		205	279[a]	93[a]	186
$HfV_2H_{0.5}D_{3.4}$	289	19.3	276	0.18		97			
$HfV_2H_{1.5}D_{2.5}$	291	19.3	280	0.22		105			
$HfV_2H_{3.0}D_{1.0}$	294	19.3	280	0.24		112			
$HfV_2H_{3.4}D_{0.5}$	294	19.3	271	0.21		141			
$ZrV_2H_{1.1}$	200	19.3	228	0.16	3.1×10^{-12}	110	256	32	224
$ZrV_2H_{2.4}$	220	19.3	233	0.22	1.9×10^{-13}	154	265	70	195
$ZrV_2H_{3.4}$	250	19.3	257	0.21	7.2×10^{-13}	155	272	87	185
$ZrV_2H_{4.0}$	298	19.3	287	0.27		185	265[a]	90[a]	175
$ZrV_2H_{5.0}$	210	20.5	217	0.17	8.5×10^{-13}	176	265	110	155
$ZrV_2H_{1.0}D_{3.0}$	300	19.3	290	0.22		130			
$ZrV_2H_{3.0}D_{1.0}$	298	19.3	289	0.27		165			

[a] Calculated for the ordered δ-phases of HfV_2H_4 and ZrV_2H_4.

Table 4. Temperatures of phase transitions, T_0, and parameters of the motional relaxation of ^{2}D in the disordered high-temperature phases.

Sample	T_0 (K)	T_{max} (K)	E_a (eV)	$(T_{1d}^{-1})^{max}$ (s^{-1})
$HfV_2D_{1.3}$	240	252	0.22	7.0
$HfV_2D_{2.1}$	210	243	0.22	8.6
$HfV_2D_{3.8}$	268	268	0.17	8.0
$HfV_2D_{3.9}$	255	263	0.18	7.4
$HfV_2H_{0.5}D_{3.4}$	289	262	0.18	9.2
$HfV_2H_{1.5}D_{2.5}$	291	263	0.18	8.6
$HfV_2H_{3.0}D_{1.0}$	294	262	0.20	8.3
$HfV_2H_{3.4}D_{0.5}$	294	262	0.18	7.8
$ZrV_2D_{1.3}$	220	238	0.22	6.5
$ZrV_2D_{2.0}$	298	263	0.25	9.0
$ZrV_2D_{3.1}$	257	262	0.25	8.7
$ZrV_2D_{3.9}$	301	294	0.23	8.5
$ZrV_2D_{4.6}$	222	234	0.13	8.6
$ZrV_2D_{5.0}$	210	224	0.14	9.6
$ZrV_2H_{1.0}D_{3.0}$	300	290	0.23	8.5
$ZrV_2H_{3.0}D_{1.0}$	298	290	0.21	9.4

estimated using equations (7) and (2) at the points of T_{1d}^{-1} maxima, if the T_{1d}^{-1} maximum occurs in the disordered phase, i.e. $T_{max} > T_0$. For the samples with $T_{max} < T_0$, the values of τ_{d0} have not been estimated.

As can be seen from table 3, the activation energy in the disordered phase of HfV_2H_x does not depend on x ($0.5 \leqslant x \leqslant 4.0$) within the experimental uncertainty of ± 0.01 eV. These results do not agree with the data of Shinar *et al* [11], who reported more than a fivefold increase in the average value of E_a between $x = 0.5$ and 4.0. The main source of the discrepancy seems to be related to the lack of an adequate treatment of phase changes in [11]. On the other hand, our E_a values for the disordered phase of HfV_2H_x are in excellent agreement with the results of recent quasi-elastic neutron scattering experiments on $HfV_2H_{3.3}$ [27].

For the disordered phase of ZrV_2H_x the value of E_a is found to increase with x changing from 1.1 to 4.0 and to decrease sharply for $x > 4$. A similar decrease in E_a for $x > 4$ is observed for ZrV_2D_x (table 4). The decrease in the activation energy at high H(D) concentrations may be attributed to the details of interstitial site occupation. It is known [3] that for $x > 3$ hydrogen atoms in $HfV_2H_x(D_x)$ and $ZrV_2H_x(D_x)$ start to occupy e-sites in addition to g-sites, the fraction of occupied e-sites increasing with H(D) content. The occupation of e-sites may result in lower values of the effective activation energies, since this is expected to introduce 'easy' diffusion paths. Our E_a values for the disordered phase of ZrV_2H_x (table 3) are in reasonable agreement with the corresponding average values of Shinar *et al* [11] for $x \simeq 1$ and $x \simeq 2.5$; however, for $3.3 \leqslant x \leqslant 4.0$ our E_a values are considerably lower than those of [11]. Shinar *et al* [11] have also reported on the existence of a narrow peak in the x dependence of E_a in ZrV_2H_x near $x = 1.6$. We have not studied the behaviour of T_1 in this concentration range. We note, however, that the sharp increase in E_a in this region, as in the vicinity of $x = 4$, may be an artifact associated with the phase transition, since the phase diagram of $ZrV_2H_x(D_x)$ [5, 6, 8–10] exhibits a T_0 maximum near $x = 2$. Comparison of our E_a results for the disordered phase of ZrV_2H_x with those obtained from quasi-elastic neutron scattering experiments [28] shows that, although the shape of the $E_a(x)$ dependence is similar in both works, our E_a values are higher.

We now consider isotope effects in E_a. Comparing the data presented in tables 3 and 4, we can conclude that at high hydrogen concentrations ($x > 3.5$) there is a distinct inverse isotope effect in the activation energy: $E_a^D < E_a^H$ for both $HfV_2H_x(D_x)$ and $ZrV_2H_x(D_x)$ systems. This sign of the isotope effect in E_a has also been found for the hydrides (deuterides) of some FCC metals including $PdH_x(D_x)$ [29]. As a result of this effect, at low temperatures τ_d^D is usually less than τ_d^H, i.e. the hopping rate of D is higher than that of H. However, in the region of low x ($x < 3$) the isotope dependence of E_a is different: $E_a^D \simeq E_a^H$ for $HfV_2H_x(D_x)$ and $E_a^D > E_a^H$ for $ZrV_2H_x(D_x)$. The change in the sign of the isotope effect in E_a with increasing H(D) content may be attributed to a difference in inequivalent site occupation for concentrated hydrides and deuterides. In fact, as noted above, the increase in e-site occupancy is expected to lead to the decrease in E_a. On the other hand, as has been discussed in [4, 5], for $HfV_2H_x(D_x)$ and $ZrV_2H_x(D_x)$ the equilibrium fraction of occupied e-sites in a deuteride should be higher than in a hydride of the same composition. Hence, the decrease in E_a with increasing x in the deuterides is expected to be stronger than in the hydrides, resulting in the inequality $E_a^D < E_a^H$ at high x.

The particularly interesting question is whether hydrogen diffusion parameters are changed when the isotope substitution is only partial. The corresponding experimental data may clarify the role of the interaction between diffusing atoms at high hydrogen

concentrations. It has been found from NMR measurements on mixed-isotope systems NbH_xD_z and TaH_xD_z [30, 31] that the diffusion of both H and D in the same sample is characterized by the same E_a value, although in binary systems NbH_{x+z} (NbD_{x+z}) and TaH_{x+z} (TaD_{x+z}) there is a considerable difference between E_a^D and E_a^H. These results have led the authors [30, 31] to the conclusion that the motion of hydrogen atoms in Nb and Ta should be strongly correlated. Our results for $HfV_2H_zD_{4-z}$ and $ZrV_2H_zD_{4-z}$ (tables 3 and 4) show that the inequality $E_a^D < E_a^H$ is retained for the diffusion of H and D in the same mixed-isotope sample, the values of $E_a^{H(D)}$ being close to the corresponding values for a fully hydrided (deuterided) compound. The exceptions are the samples with low z ($HfV_2H_{0.5}D_{3.5}$ and $ZrV_2H_{1.0}D_{3.0}$), for which the difference between E_a^D and E_a^H is within experimental uncertainty. Thus, our results do not support the existence of strong correlation between the motion of hydrogen isotopes in the disordered concentrated solutions $HfV_2H_zD_{4-z}$ and $ZrV_2H_zD_{4-z}$.

We now consider the maximum values of T_{1d}^{-1} for protons. It follows from equation (2) that $(T_{1d}^{-1})^{max}$ is determined by the values of M_{2H} and M_{2M}, which can be calculated for the known structure from equations (3) and (4). In the last four columns of table 3 the observed values of $(T_{1d}^{-1})^{max}$ are compared with the calculated ones, including the contributions from HH and HV dipolar interactions. We have assumed random g-site occupation restricted by blocking effects [32, 33], preventing simultaneous occupation of tetrahedra having a common face. For $HfV_2H_{4.0}$ and $ZrV_2H_{4.0}$ the value of $(T_{1d}^{-1})^{max}$ was calculated for the ordered δ-phase [1, 2], since for these compounds the T_{1d}^{-1} maximum is observed at $T_{max} < T_0$. As can be seen from table 3, for all the studied compounds the calculated values of $(T_{1d}^{-1})^{max}$ are considerably higher than the observed ones. We now discuss the possible sources of this discrepancy.

In the framework of the model employing the double-peaked distribution of τ_d (or E_a) the value of $(T_{1d}^{-1})^{max}$ may be lower than the one calculated from equations (2)–(4) since a certain fraction of dipole–dipole interactions is already averaged out due to an additional motional process at low temperatures (see e.g. [18]). However, as will be shown in the next section, the relative amplitude of the additional peak is expected to be small (~10% of the amplitude of the main peak). Therefore, the additional motional process cannot be responsible for more than a twofold discrepancy between the observed and calculated values of $(T_{1d}^{-1})^{max}$ for some x.

The dominant contribution to the calculated values of $(T_{1d}^{-1})^{max}$ results from HV interactions, especially at low hydrogen concentrations. The HV contribution does not depend on the mutual configuration of H atoms. Hence, the use of some other models of hydrogen configuration would hardly reduce the discrepancy. Allowance for the partial occupation of e-sites for $x > 3$ would only result in the further increase of the calculated values of $(T_{1d}^{-1})_{HV}^{max}$.

The analysis of the data presented in table 3 has led us to the conclusion that the main source of the discussed discrepancies is the overestimated value of the contribution $(T_{1d}^{-1})_{HV}$ calculated from equations (2) and (4). In fact, the experimental estimate of $(T_{1d}^{-1})_{HV}^{max}$ can be obtained by extrapolating the concentration dependence of $(T_{1d}^{-1})^{max}$ to $x = 0$. The corresponding values of $(T_{1d}^{-1})_{x\to 0}^{max}$ are equal to $70\,s^{-1}$ (HfV_2H_x, $\omega/2\pi = 20.5$ MHz) and $85\,s^{-1}$ (ZrV_2H_x, $\omega/2\pi = 19.3$ MHz), being considerably lower than the calculated values of $(T_{1d}^{-1})_{HV}^{max}$. On the other hand, the calculated contribution $(T_{1d}^{-1})_{HH}^{max}$ appears to have the correct value, as can be derived from the x dependence of $(T_{1d}^{-1})_{obs}^{max}$ in HfV_2H_x and ZrV_2H_x and from the z dependence of $(T_{1d}^{-1})_{obs}^{max}$ in $HfV_2H_zD_{4-z}$ and $ZrV_2H_zD_{4-z}$. It should be noted that similar discrepancies between the observed and calculated values of $(T_{1d}^{-1})_{HM}^{max}$ in NbH_x [34] and TaH_x [35] have been ascribed [35] to

Table 5. Parameters of hydrogen motion in the ordered low-temperature phases δ-HfV_2H_4, δ-ZrV_2H_4 and β-ZrV_2D_2 in terms of the double-peaked model.

Sample	$\bar{E}_{a1}$ (eV)	$\bar{E}_{a2}$ (eV)	ΔE_{a2} (eV)	τ_{d0} (s)	A
δ-HfV_2H_4	0.29	0.22	0.084	6.6×10^{-14}	0.065
δ-ZrV_2H_4	0.36	0.28	0.10	3.9×10^{-15}	0.074
β-ZrV_2D_2	0.26	0.20	0.074	1.4×10^{-13} [a]	0.10

[a] Assuming that the quadrupolar contribution to the relaxation rate is proportional to the dipolar one.

the effects of quadrupole interaction on metal nuclei, resulting in the reduction of the actual dipolar HM contribution to T_{1d}^{-1} with respect to that calculated from equations (2) and (4). The $(T_{1d}^{-1})^{max}$ data for HfV_2H_x and ZrV_2H_x may also be interpreted in an analogous way, since in these systems ^{51}V nuclei are known to possess a strong quadrupole interaction [36–38].

4.4. Parameters of H(D) diffusion in the ordered phases

As noted above, the nuclear spin relaxation data for $HfV_2H_x(D_x)$ and $ZrV_2H_x(D_x)$ can be described in terms of the model using a double-peaked distribution of E_a. The corresponding normalized distribution function is given by [14]

$$G(E_a) = (1 - A)\delta(\bar{E}_{a1} - E_a) + AG_2(\bar{E}_{a2}, E_a, \Delta E_{a2}) \tag{9}$$

where $\bar{E}_{a2} < \bar{E}_{a1}$, and usually $A \ll 1$. For G_2 it is convenient to choose the Gaussian centred on $\bar{E}_{a2}$ and having a full width at half-maximum ΔE_{a2}. The characteristic features of the double-peaked model are most distinctly manifested in the behaviour of relaxation rates below T_{max}. However, the applicability of this model to analysis of the relaxation data for the low-temperature phases of $HfV_2H_x(D_x)$ and $ZrV_2H_x(D_x)$ is somewhat restricted, since for most of the samples $T_0 < T_{max}$, and thus the temperature range of the analysis is rather narrow. Therefore, the parameters of H(D) motion in the ordered phases have been evaluated only for the three samples, $HfV_2H_{4.0}$, $ZrV_2H_{4.0}$ and $ZrV_2D_{2.0}$, having the highest ordering temperatures. For these samples $T_0 > T_{max}$.

The results of the fitting of the double-peaked model to the $T_{1d}^{-1}(T)$ data for $HfV_2H_{4.0}$ at different frequencies are shown as full curves in figure 5. The model calculations are based on equations (2), (7), (8) and (9), the second moments being chosen to fit the observed maximum T_{1d}^{-1} values. The parameters $\bar{E}_{a1}$, $\bar{E}_{a2}$, ΔE_{a2}, τ_{d0} and A are varied until the best fit to all the relaxation data at different frequencies is obtained; the resulting fitting parameters are given in table . As can be seen from figure 5, and model employing a double-peaked distribution of E_a gives a satisfactory description of the main experimental features in a wide frequency range.

The results of analogous fittings to the $T_{1d}^{-1}(T)$ data for $ZrV_2H_{4.0}$ and $ZrV_2D_{2.0}$ are shown as full curves in figures 3 and 8, respectively. The fitting parameters for these compounds are included in table 5. In all the studied cases the relative amplitude of the low-E_a peak is small. This peak has a negligible effect on the relaxation rate behaviour at temperatures near and above the T_1^{-1} maximum. The relative width of the low-E_a peak, $\Delta E_{a2}/\bar{E}_{a2}$, is found to be in the range 0.35–0.38. It is interesting to compare the

activation energies $\tilde{E}_{a1}$, corresponding to the high-E_a peak in the ordered phases, with the E_a values for the disordered phase of the same compounds listed in table 3 and 4. The comparison shows that H(D) ordering is accompanied by the increase in the activation energy, i.e. the diffusion of H(D) in the ordered phase requires higher activation energy than in the disordered phase.

The nature of the two frequency scales of H(D) motion in $HfV_2H_x(D_x)$ and $ZrV_2H_x(D_x)$ remains to be elucidated. In the ordered phases of $HfV_2H_4(D_4)$ and $ZrV_2H_4(D_4)$ the diffusion mechanism may be analogous to the one reported for β-V_2H [39]. The 'slow' (high-E_a) process may correspond to H(D) hopping between the nearly filled and the nearly empty sublattices of g-sites. The 'fast' (low-E_a) process may be due to the motion of a small fraction of H(D) atoms over the nearly empty sublattice of g-sites. The alternative explanation implies the coexistence of long-range diffusion with some kind of fast localized motion.

5. Conclusions

The main results of our NMR studies of H(D) motion in $HfV_2H_x(D_x)$ and $ZrV_2H_x(D_x)$ may be summarized as follows.

Considerable deviations from the Korringa-type behaviour of the proton spin–lattice relaxation rates are observed even below 100 K. Hence, in order to determine the electronic contribution to T_1^{-1} reliably, it is crucial to make measurements down to liquid-helium temperatures and at high frequencies.

Phase transformations are found to have strong effects on the H(D) diffusion parameters. These effects are especially pronounced for compounds with $x = 4$ corresponding to the stoichiometric composition of the ordered δ-phase. The H(D) ordering results in the increase of τ_d values.

For the disordered (high-temperature) phases of $HfV_2H_x(D_x)$ and $ZrV_2H_x(D_x)$ the experimental data can be reasonably described in terms of the usual BPP model with a single activation energy E_a. In HfV_2H_x, E_a is nearly constant in the range $0.5 \leqslant x \leqslant 4.0$; and in ZrV_2H_x, the activation energy increases with x changing from 1.1 to 4.0 and starts to decrease at $x > 4.0$. For both systems at $x > 3.5$ there is a distinct isotope effect in E_a for the disordered phase: $E_a^D < E_a^H$. At lower concentrations the isotope effect decreases and even changes sign for $ZrV_2H_x(D_x)$. This kind of behaviour may arise from differences in g- and e-site occupancy between the concentrated hydrides and deuterides.

For the ordered (low-temperature) phases of $HfV_2H_x(D_x)$ and $ZrV_2H_x(D_x)$ the experimental data can be described in terms of the model using a double-peaked distribution of E_a values. This model implies the coexistence of two types of H(D) motion with different frequency scales. Such a coexistence appears to be a common feature of a number of Laves-phase hydrides [12, 14, 18, 28]. The nature of the two frequency scales of H(D) motion remains to be elucidated.

References

[1] Irodova A V, Glazkov V P, Somenkov V A and Shil'shtein S Sh 1980 *Sov. Phys.–Solid State* **22** 45
[2] Didisheim J J, Ivon K, Fischer P and Tissot P 1981 *Solid State Commun.* **38** 637
[3] Somenkov V A and Irodova A V 1984 *J. Less-Common Met.* **101** 481
[4] Skripov A V, Belyaev M Yu, Kozhanov V N, Stepanov A P, Kost M E and Padurets L N 1986 *Solid State Commun.* **57** 249

[5] Belyaev M Yu, Skripov A V, Stepanov A P, Kost M E and Padurets L N 1986 *Sov. Phys.–Solid State* **28** 1538
[6] Irodova A V, Borisov I I, Lavrova O A, Laskova G V, Padurets L N and Pripadchev S A 1983 *Sov. Phys.–Solid State* **25** 747
[7] Geibel C, Goldacker W, Keiber H, Oestreich V, Rietschel H and Wühl H 1984 *Phys. Rev.* B **30** 6363
[8] Irodova A V, Lavrova O A, Laskova G V, Kost M E, Padurets L N and Shilov A L 1988 *Zh. Neorg. Khim.* **33** 1879
[9] Vajda P, Daou J N, Burger J P, Shaltiel D and Grayevsky A 1989 *Z. Phys. Chem. NF* **163** 75
[10] Hempelmann R, Richter D, Hartman O, Karlsson E and Wäppling R 1989 *J. Chem. Phys.* **90** 1935
[11] Shinar J, Davidov D and Shaltiel D 1984 *Phys. Rev.* B **30** 6331
[12] Bowman R C, Craft B D, Attalla A and Johnson J R 1983 *Int. J. Hydrogen Energy* **8** 801
[13] Morimoto K, Saga M, Fujii H, Okamoto T and Hihara T 1988 *J. Phys. Soc. Japan* **57** 647
[14] Skripov A V, Rychkova S V, Belyaev M Yu and Stepanov A P 1989 *Solid State Commun.* **71** 1119
[15] Belyaev M Yu, Skripov A V, Kozhanov V N and Stepanov A P 1984 *Sov. Phys.–Solid State* **26** 1285
[16] Skripov A V, Belyaev M Yu, Rychkova S V and Stepanov A P 1987 *Fiz. Tverd. Tela* **29** 3160
[17] Kirchheim R and Huang X Y 1987 *Phys. Status Solidi* b **144** 253
[18] Skripov A V, Belyaev M Yu, Rychkova S V and Stepanov A P 1989 *J. Phys.: Condens. Matter* **1** 2121
[19] Abragam A 1961 *The Principles of Nuclear Magnetism* (Oxford: Clarendon) ch VIII
[20] Bloembergen N, Purcell E M and Pound R M 1948 *Phys. Rev.* **73** 679
[21] Faux D A, Ross D K and Sholl C A 1986 *J. Phys. C: Solid State Phys.* **19** 4115
[22] Seymour E F W 1982 *J. Less-Common Met.* **88** 323
[23] Salibi N, Ting B, Cornell D and Norberg R E 1988 *Phys. Rev.* B **38** 4416
[24] Belyaev M Yu, Skripov A V, Stepanov A P and Galoshina E V 1987 *Fiz. Metal. Metalloved.* **63** 905
[25] Stepanov A P, Skripov A V and Belyaev M Yu 1989 *Z. Phys. Chem. NF* **163** 603
[26] Shinar J 1984 *J. Less-Common Met.* **104** 125
[27] Havill R L, Titman J M, Wright M S and Crouch M A 1989 *Z. Phys. Chem. NF* **164** 1083
[28] Schönfeld C, Schätzler R and Hempelmann R 1989 *Ber. Bunsenges. Phys. Chem.* **93** 1326
[29] Völkl J and Alefeld G 1978 *Hydrogen in Metals I* ed G Alefeld and J Völkl (Berlin: Springer) p 321
[30] Fukai Y, Kubo K and Kazama S 1979 *Z. Phys. Chem. NF* **115** 181
[31] Kazama S and Fukai Y 1980 *Proc. Int. Symp. JIMIS-2: Hydrogen in Metals (Sendai)* p 173
[32] Switendick A C 1979 *Z. Phys. Chem. NF* **117** 89
[33] Shoemaker D P and Shoemaker C B 1979 *J. Less-Common Met.* **68** 43
[34] Zamir D and Cotts R M 1964 *Phys. Rev.* **134** A666
[35] Pedersen B, Krogdahl T and Stokkeland O E 1965 *J. Chem. Phys.* **42** 72
[36] Peretz M, Barak J, Zamir D and Shinar J 1981 *Phys. Rev.* B **23** 1031
[37] Ding D T, de Lange J I, Klaassen T O, Poulis N J, Davidov D and Shinar J 1982 *Solid State Commun.* **42** 137
[38] Skripov A V, Belyaev M Yu and Stepanov A P 1989 *Solid State Commun.* **71** 321
[39] Richter D, Mahling-Ennaoui S and Hempelmann R 1989 *Z. Phys. Chem. NF* **164** 907